RSC Advances

PAPER

View Article Online
View Journal | View Issue

Cite this: *RSC Adv.*, 2016, **6**, 2793

A simple and low-cost fully 3D-printed non-planar emulsion generator†

Jia Ming Zhang,[a] Er Qiang Li,[a] Andres A. Aguirre-Pablo[a] and Sigurdur T. Thoroddsen*[ab]

Droplet-based microfluidic devices provide a powerful platform for material, chemical and biological applications based on droplet templates. The technique traditionally utilized to fabricate microfluidic emulsion generators, *i.e.* soft-lithography, is complex and expensive for producing three-dimensional (3D) structures. The emergent 3D printing technology provides an attractive alternative due to its simplicity and low-cost. Recently a handful of studies have already demonstrated droplet production through 3D-printed microfluidic devices. However, these devices invariably use purely two-dimensional (2D) flow structures. Herein we apply 3D printing technology to fabricate simple and low-cost 3D miniaturized fluidic devices for droplet generation (single emulsion) and droplet-in-droplet (double emulsion) without need for surface treatment of the channel walls. This is accomplished by varying the channel diameters at the junction, so the inner liquid does not touch the outer walls. This 3D-printed emulsion generator has been successfully tested over a range of conditions. We also formulate and demonstrate, for the first time, uniform scaling laws for the emulsion drop sizes generated in different regimes, by incorporating the dynamic contact angle effects during the drop formation. Magnetically responsive microspheres are also produced with our emulsion templates, demonstrating the potential applications of this 3D emulsion generator in chemical and material engineering.

Received 3rd November 2015
Accepted 21st December 2015

DOI: 10.1039/c5ra23129a

www.rsc.org/advances

1 Introduction

Droplet-based microfluidics provides a powerful approach to generate and manipulate monodisperse droplets or bubbles in a continuous liquid phase,[1] and has undergone a rapid growing in recent years, due to its great potential in material, chemical and biological applications.[2–7] One of the successful extensions of droplet-based microfluidics is the generation of multiple emulsion droplets, which provide viable templates for producing various types of microcapsules or microgels.[8,9] To extend droplet-based microfluidics for practical uses in industry, it is crucial to develop current fabrication techniques in a simple, rapid and low-cost manner.

A well-known fabrication technique for microfluidic devices is soft-lithography.[10] Polydimethylsiloxane (PDMS) is used as replica from an original hard master to fabricate microchannels where the hard master is usually produced by photolithography technique. This two-step process is normally time-consuming and requires expensive facilities in a clean room as well as complex skills and operations. In addition, it is complex to control the wettability of channel walls,[11] which is crucial for stable production of droplets, especially for multiple emulsion droplets.[12] Also, the complications mentioned previously make the mass production of microfluidic devices difficult and expensive for industry applications.

To produce controllable double emulsions, Weitz's group[13] developed a microfluidic device based on capillary tubes. These kind of glass microfluidic devices have become popular due to their chemical robustness and ease of modifying their surface wettability, compared to the soft-lithography technique. Higher-order multiple emulsions or bubble emulsions can also be produced based on this type of microfluidic devices.[14–17] However, tapered glass capillaries and later assembly needs to be done manually. In essence this means that each device is custom made, which does not assure production repeatability and makes it difficult to fabricate in the large quantities required in industrial applications.

An alternative low-cost technique for soft-lithography is micromolding of thermoplastic polymers such as poly-methylmetacrylate (PMMA), which is widely used in micro-fluidics research.[18–20] It does not require high-cost equipments and avoids complex processes. However, this surface machining technique cannot easily fabricate three-dimensional (3D)

[a]*Division of Physical Sciences and Engineering, King Abdullah University of Science and Technology (KAUST), Thuwal, 23955-6900, Saudi Arabia. E-mail: sigurdur.thoroddsen@kaust.edu.sa*

[b]*Clean Combustion Research Center, King Abdullah University of Science and Technology (KAUST), Thuwal, 23955-6900, Saudi Arabia*

† Electronic supplementary information (ESI) available: (S1) resin testing, (S2) single W/O emulsion, (S3) single O/W emulsion, (S4) double O/W/O emulsion, (S5) double W/O/W emulsion, (S6) double air/O/W emulsion. See DOI: 10.1039/c5ra23129a

structures. Furthermore, similar to the soft-lithography technique, it is difficult to control the wettability of the channel wall, which limits its applications in droplet-based microfluidics.

In recent years, a variety of 3D printing technologies have achieved great progress and made it possible to produce operational devices, such as microbatteries,[21] scaffolds,[22] microvascular networks[23] and reactionware.[24] This additive manufacturing technology has the potential to greatly reduce ecological footprints as well as the energy consumed in manufacturing. Also it is a data-driven process that patterns directly onto the substrate with ejection.[25] Due to its simple and low-cost fabrication process, 3D printing technology has recently been applied to fabricate miniaturized devices.[26–30] However, few researchers have applied 3D printing technology to fabricate droplet generators, and so far, still employ the traditional planar structures to produce droplets,[31–33] not taking advantage of 3D flow structure that can be easily produced by 3D printing technology for generating droplets. Following the elegant non-planar structure design by Rotem *et al.*[34] to generate droplets using the soft-lithography technique, here we report design and fabrication of simple and low-cost 3D-printed emulsion generator devices, without need for surface treatment of the channel walls. Such treatment is not needed, due to the local 3D geometry of the junctions where emulsion droplets are produced. This 3D geometry of junctions can be printed through current 3D-printing technique but is difficult to achieve when using the conventional fabrication techniques. We have investigated droplet production in our 3D droplet generators and illustrated their feasibility for stable single and multiple emulsions production. Single emulsions, water-in-oil (W/O) or oil-in-water (O/W), as well as double emulsions, water-in-oil-in-water (W/O/W), oil-in-water-in-oil (O/W/O) or air-in-oil-in-water (air/O/W) can be successfully produced by the same emulsion generator without surface wettability treatment. The simple fabrication process involves design using Computer Aided Design (CAD) software and printing using an inexpensive commercial desktop 3D printer. The total cost of materials for one generator is below $1. The whole printing process only takes a couple of hours. This capability could be highly convenient for researchers, especially for those not familiar with complicated fabrication skills, to design and fabricate customized miniaturized devices rapidly. Furthermore, uniform scaling laws for prediction of emulsion (W/O and O/W) droplet sizes generated in different regimes are successfully proposed. Finally, we produce magnetic particles based on droplet templates, demonstrating the extensive possibilities of chemical and material applications through our 3D-printed miniaturized devices.

2 Materials and methods

Emulsion droplet generators are designed using Solidworks (Dassault Systemes S.A.), and then fabricated with Form 1+ printer (Formlabs, Inc.) as shown in Fig. 1(a). The printer only costs $2799 and is based on the stereolithography technique to build structures.[35] The great advantage of this technique applied in microfluidics lies in the clear resin provided for printing, which provides an excellent transparency and thus allows researchers to observe the internal fluid field and develop variety of microfluidic applications requiring optical access.

In addition, the Young's modulus of postcured clear resin is 2.7 Gpa, much larger than that of PDMS: 0.75×10^{-3} Gpa. Thus, our devices printed by this material are capable of withstanding high liquid flow rate and input pressure.

This clear resin contains modified acrylate oligomer and monomer, together with a photoinitiator and their weight ratio is propriety. More details can be found in the ESI, S1.†

The basic geometry of our emulsion generator is illustrated in Fig. 1(b). The center inlet with diameter $D_I = 600$ μm introduces the inner dispersed phase Q_I, whereas two side inlets with diameter $D_S = 1000$ μm introduce the outer continuous phase Q_O. Both inner and outer phase flow out through the outlet with diameter $D_O = 1000$ μm. The center inlet is smaller than the side inlets, forming a 3D junction where the inner phase is pinched-off to generate droplets without touching the downstream walls. This 3D junction thereby allows the outer phase coming from the side inlets to encapsulate the inner phase completely when the flow rate of outer phase is large enough, which prevents the inner phase from contacting the channel walls. Consequently, the drop formation at the junction will not be affected by the channel wall wetting conditions. Therefore, the complicated process of local surface treatment on channel walls is avoided. Both single emulsions of W/O and O/W, are successfully produced in the same emulsion generator without any surface treatment.

Subsequently, we extend this single 3D junction to two sequential junctions for double emulsion production. As shown in Fig. 1(c), the inner channel with diameter $D_I = 600$ μm carries the inner phase to the first junction. The middle channel with diameter $D_M = 1000$ μm carries the middle phase also to the first junction to pinch off the inner phase and generate inner droplets. Then the inner droplets and middle phase are carried to the second junction, where the outer phase carried by the outer channel with diameter $D_O = 2000$ μm squeezes the middle phase and generate outer droplets. All three phases are collected in the outlet channel with diameter 2000 μm. Due to the gradual increase of channel diameter from inner to outer, both the inner phase in the first junction and the middle phase in the second junction are prevented from contacting the channel walls. Thus, different double emulsions (W/O/W, O/W/O and air/O/W) can be generated using the same chip without the need to modify the wettability of the channel walls. Such special 3D structure will require complicated fabrication processes with high-cost equipment and skilled people for traditional fabrication techniques, but it can be simply and inexpensively fabricated through 3D printing technology.

Syringe needles are inserted into the openings in the chip, sealed by epoxy to form inlets and outlet. Meanwhile, we design and print a cone inlet, which can be directly connected with tubes for liquid input as shown in Fig. 1(c). Silicone oil (Sigma-Aldrich Corp.) of different viscosities are employed as the oil phases, and water–glycerin mixtures of different viscosities are employed as aqueous phases. Red dyes are applied in the

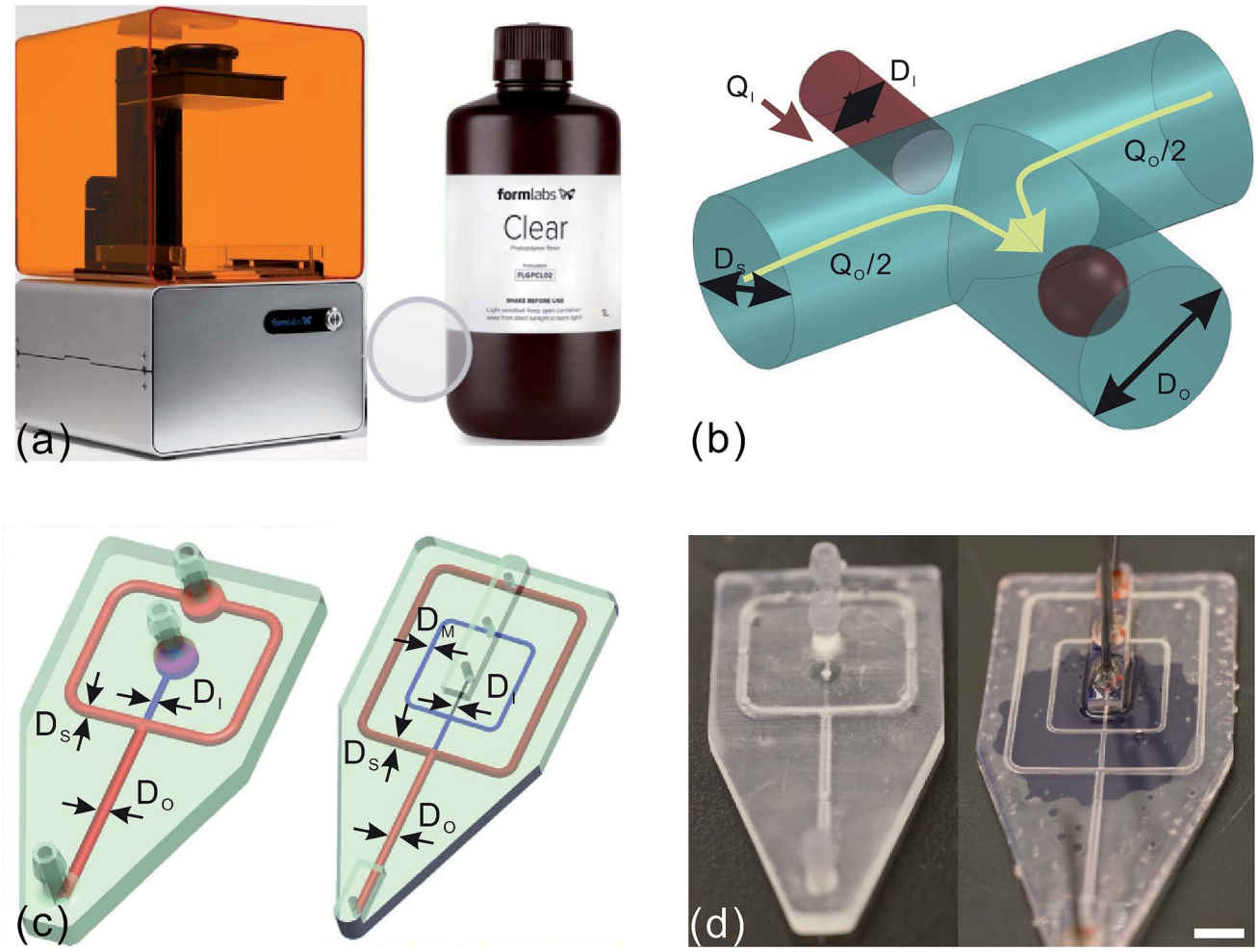

Fig. 1 (a) Photograph of the Form 1+ printer with its clear resin, used to fabricate our emulsion generator. (b) Local 3D structure design for emulsion generation. The inner phase (Q_I) flows in the central inlet channel with diameter $D_I = 0.6$ mm. The outer phase (Q_O) flows in the two side channels with diameter $D_S = 1$ mm. These two phases flow together into the outlet channel with diameter $D_O = 1$ mm. (c) Schematics of single and double emulsion generator. For double emulsion generator, the dimensions are $D_I = 0.6$ mm, $D_M = 1$ mm and $D_O = 2$ mm. (d) 3D-printed single and double emulsion generators. Scale bar is 1 cm.

aqueous phase to enhance observation. Up to three syringe pumps (Fusion 200, Chemyx, Inc.) are applied for driving the fluids into the generators. The formation process of the emulsion droplets are observed and recorded with a high-speed CMOS video camera SA-3. The sizes of the emulsion droplets are analyzed using free image-analysis software ImageJ.

All experiments are carried out at room temperature (22 °C).

3 Results

First, we choose different viscosities of silicone oil listed in Table 1 as the outer continuous phase and 20 cP water–glycerin mixture as the inner disperse phase, to generate W/O emulsions as shown in Fig. 2(a), and also seen in ESI, S2.† Since our printing material has a higher affinity for the oil phase, the inner aqueous phase can be easily encapsulated by the outer oil phase. With the flow rate ratio alteration, two regimes, dripping and jetting, are observed.[36] The dynamic contact angle of inner aqueous phase during the drop formation, $\theta \sim 82°$, as shown in Fig. 2(a).

After successful generation of W/O emulsions, we use the same generator to also generate O/W emulsions as shown in Fig. 2(b), and also seen in ESI, S3.† Different viscosities of water–glycerin mixture listed in Table 1 are used as outer aqueous phase respectively and 20 cSt silicone oil is used as inner oil phase. Before O/W emulsion generation, isopropyl alcohol and DI water are used to flush the channels for 10 minutes to remove the oil residues and water–glycerin mixture is pumped into the chip first. Then, the inner silicone oil is injected into the chip. We always keep the inner oil phase flow rate (Q_I) less than the outer aqueous phase flow rate (Q_O), $Q_{I,max} \approx 0.35Q_O$, to prevent the inner oils phase from wetting the channel walls. Once the inner oil contacts the channel walls and form an oil film on the walls, oil drops cannot be produced anymore. No dripping or jetting regime is observed in O/W emulsion generation, while an oil cap as shown in Fig. 2(b) is completely surrounded by the outer aqueous phase and pinched-off to generate droplets. The dynamic contact angle of

Table 1 Viscosities of the different liquids used in our experiments for generation of single and double emulsions[a]

W/O		O/W		W/O/W			O/W/O			Air/O/W		
Inner	Outer	Inner	Outer	Inner	Middle	Outer	Inner	Middle	Outer	Inner	Middle	Outer
20	50	20	50	20	500	1000	20	500	1000	Nitrogen	500	500
20	100	20	100	—	—	—	—	—	—	—	—	—
20	350	20	350	—	—	—	—	—	—	—	—	—

[a] W: water–glycerin mixture, unit: cP; O: silicone oil, unit: cSt.

inner oil phase during the drop formation, $\theta \sim 70^\circ$, as shown in Fig. 2(b).

We have carried out two series of experiments for both W/O and O/W emulsion droplet production. (1) Keeping the inner phase flow rate constant and increase the outer phase flow rate until the inner phase fails to flow out from the inner channel due to the high shear exerted by outer liquid phase; (2) keeping the outer phase flow rate constant and increase the inner phase flow rate until the inner phase contacts the channel wall and no droplet can be generated. In the first series of experiments, we keep the inner phase flow rate constant as 30 μL min^{-1}, and increase the outer phase flow rate from 200 μL min^{-1} to 2000 μL min^{-1}. With the increase of the outer phase flow rate, droplet generation sizes decrease, as depicted in Fig. 3. Under the same flow rate ratio, smaller droplets are generated with the higher outer phase viscosity, because higher viscosity introduces higher shear-stress to the inner phase and make it pinch off more easily to generate smaller droplets.

In the second series of experiments, we keep the outer phase flow rate constant for each viscosity of the outer oil phase: [900 μL min^{-1} for 50 cSt; 700 μL min^{-1} for 100 cSt; 500 μL min^{-1} for 350 cSt] for the W/O emulsion, and for each viscosity of the outer aqueous phase: [900 μL min^{-1} for 50 cP; 650 μL min^{-1} for 100 cP; 300 μL min^{-1} for 350 cP] for the O/W emulsion. With the increase of inner phase flow rate, droplet generation sizes increase, as depicted in Fig. 4.

In addition, as shown in Fig. 4, oil drops (solid symbol) cannot be generated when $Q_I/Q_O > 0.4$, because the oil cap has grown so big that it contacts the channel walls, which prevents the drop generation. On the other hand, aqueous drops (open symbol) can still be generated beyond this flow rate ratio, because the inner aqueous phase is in the jetting regime and droplets can also be generated downstream. This difference originates from the different droplet generation mechanism due to different wetting conditions for the inner phase.

The most relevant nondimensional parameters for multiphase flow in microfluidics, are the Reynolds number ($Re = \rho UD/\mu$) and capillary number ($Ca = \mu U/\sigma$), where U and D are the characteristic velocity and length scale; ρ, μ and σ are density, viscosity and interfacial tension between the liquids, respectively. In the first series of experiments with small constant inner phase flow rate, the Reynolds number of inner phase is much smaller than unity ($Re \ll 1$), which means the inertial forces can be ignored compared with the viscous forces. The range of outer phase capillary number from 0.01 to 1 (Ca: 0.01–1), means that the surface tension is dominant or comparable with the viscous forces. According to these facts and considering the contact angle effect on the drop formation, we propose a uniform scaling law for prediction droplet sizes generated in our 3D emulsion generator of both emulsion (W/O and O/W). This scaling is based on the method used by Cubaud and Mason,[37] who studied the dripping droplet size in

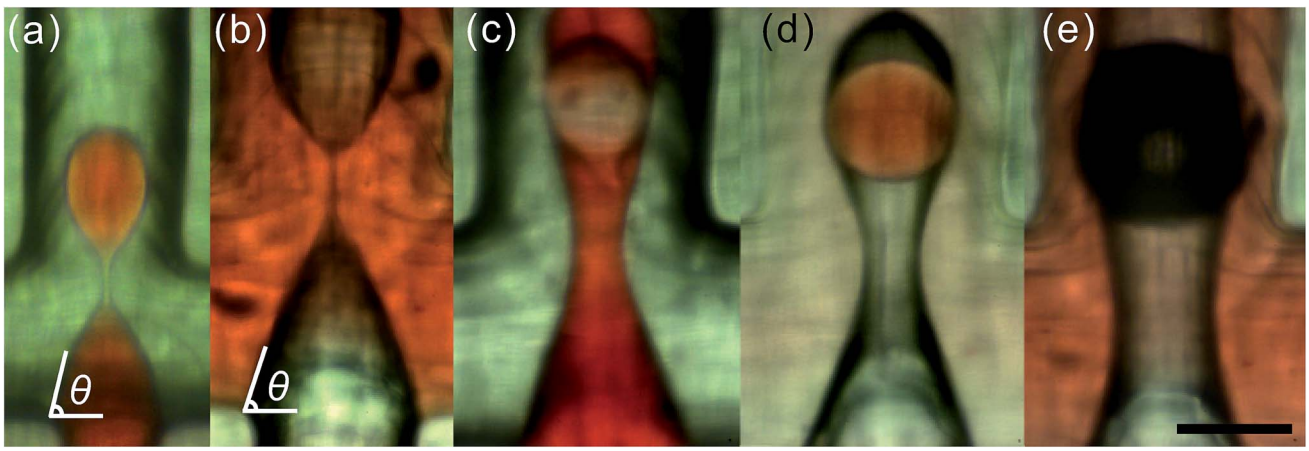

Fig. 2 Different composite emulsions generated in our devices. (a) Single W/O emulsion, (b) single O/W emulsion, (c) double O/W/O emulsion, (d) double W/O/W emulsion and (e) double air/O/W emulsion. For inner aqueous phase, the dynamic contact angle is $\theta \sim 82^\circ$; for inner oil phase, $\theta \sim 70^\circ$. Red dyes are used in the aqueous phase. Scale bar is 1 mm.

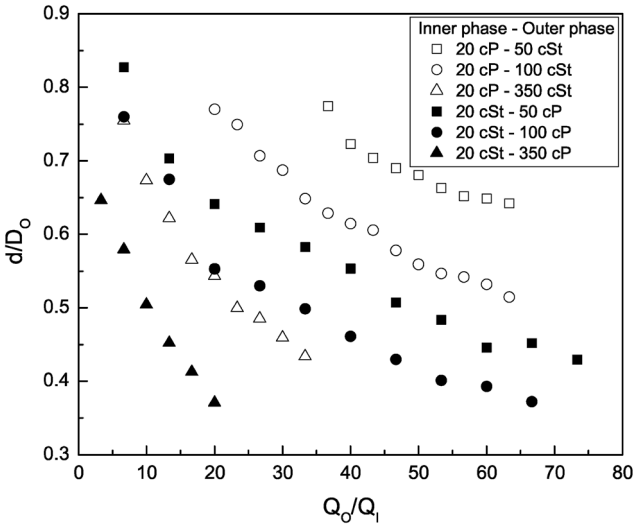

Fig. 3 Aqueous (open symbol) and oil (solid symbol) emulsion droplet diameter (d) scaled by the diameter of outlet channel (D_O) as a function of liquid flow rate ratio (Q_O/Q_I). The two different emulsions are generated in the same emulsion generator with the same constant inner phase flow rate $Q_I = 30$ μL min^{-1} while increasing the outer phase flow rate Q_O from 200 μL min^{-1} to 2000 μL min^{-1}. Liquid choices are listed in Table 1.

a 2D planar cross junction. We incorporate the dynamic contact angle effects and get $d/D_O = m[\alpha(\mathrm{Ca} \times \cos\theta)]^n$, where m and n are coefficients to be determined and $\alpha = Q_O/(Q_O + Q_I)$ is the volume fraction of outer liquid. θ is the dynamic contact angle of inner phase during the drop pinch-off. D_O is the outlet

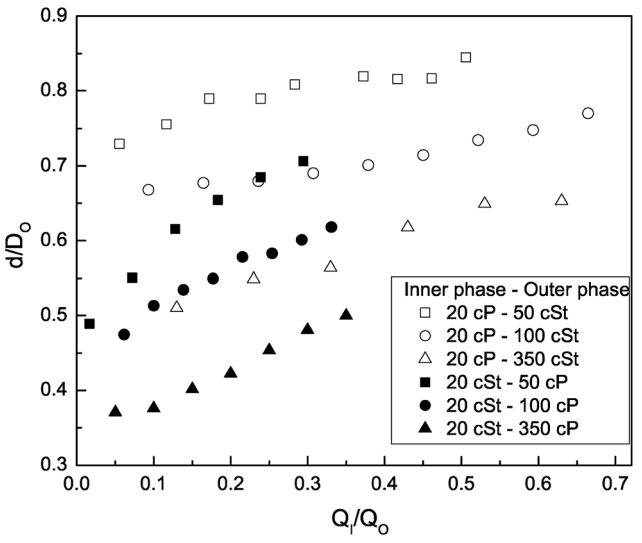

Fig. 4 Aqueous (open symbol) and oil (solid symbol) emulsion droplet diameter (d) scaled by the diameter of outlet channel (D_O) as a function of liquid flow rate ratio (Q_I/Q_O). Two different emulsions are generated in the same emulsion generator with the constant outer phase flow rate Q_O. For W/O emulsions, [$Q_O = 900$ μL min^{-1} for 50 cSt, $Q_O = 700$ μL min^{-1} for 100 cSt, $Q_O = 500$ μL min^{-1} for 350 cSt]; for O/W emulsions, [$Q_O = 900$ μL min^{-1} for 50 cP, $Q_O = 650$ μL min^{-1} for 100 cP, $Q_O = 300$ μL min^{-1} for 350 cP]. Liquid choices are listed in Table 1.

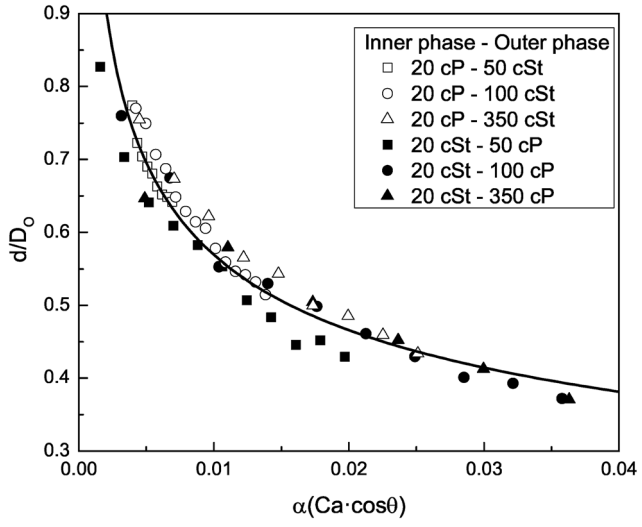

Fig. 5 Aqueous (open symbol) and oil (solid symbol) emulsion droplet diameter as a function of $\alpha(\mathrm{Ca} \times \cos\theta)$, where θ is the dynamic contact angle of inner phase during drop formation. $\theta \approx 82°$ for aqueous inner phase, and $\theta \approx 70°$ for oil inner phase.

channel diameter. In our study, $\mathrm{Ca} = \mu_O U_O/\sigma$, where μ_O is the viscosity of outer phase, σ is the interfacial tension between the inner phase (water–glycerin mixture) and outer phase (silicone oil): 40 mN m^{-1} and $U_O = Q_O/(\pi D_O^2/4)$ is the outer phase flow velocity in the outlet channel. The best fit with experimental results gives a value of $m = 0.15$ and $n = -0.29$, as shown in Fig. 5 and eqn (1). The negative exponent of Ca agrees with the fact that the viscous force favors the inner phase pinch-off and decrease the droplet size, while interfacial tension holds back the inner phase and acts against its pinch-off and increases the droplet size.

$$d/D_O = 0.15(\alpha \times \mathrm{Ca} \times \cos\theta)^{-0.29} \quad (1)$$

The mechanism is a little different in the second series of experiments. When we keep increasing the inner aqueous phase flow rate, the Reynolds number of inner phase approaches unity, which means the inertia of inner phase is comparable to the viscous force, and thus we cannot ignore this inertia in this case. Therefore, we must add Re to our scaling law here, as depicted in Fig. 6 and eqn (2).

Here $\mathrm{Re} = \rho_I U_I D_I/\mu_O$, where ρ_I is the density of inner phase, D_I is the inner channel diameter, and $U_I = Q_I/(\pi D_I^2/4)$ is the inner phase flow velocity in the inner channel. The positive exponent of Re agrees with the fact that the inertial force increases the inner phase pinch-off time and thus increases the droplet size.

$$d/D_O = 0.50[\mathrm{Re}/(\alpha \times \mathrm{Ca} \times \cos\theta)]^{0.11} \quad (2)$$

As we described in the introduction, successful double emulsion production in microfluidic devices has made a great advance in droplet-based microfluidics. Conventionally fabricated 2D channels usually require delicate control of wall

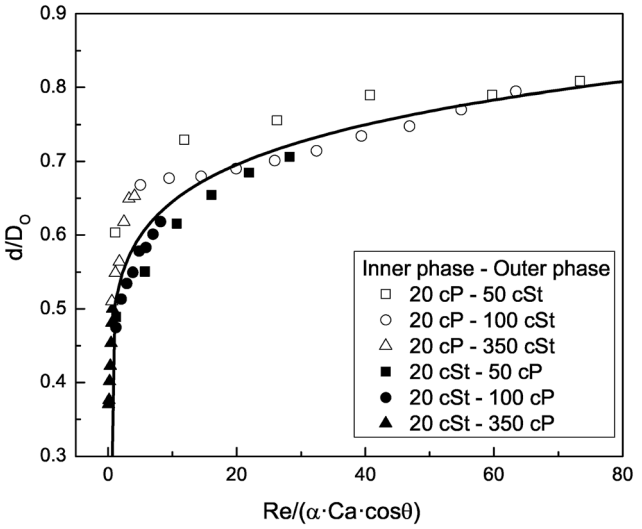

Fig. 6 Aqueous (open symbol) and oil (solid symbol) emulsion droplet diameter as a function of $Re/(\alpha \times Ca \times \cos\theta)$, where θ is the dynamic contact angle of inner phase during drop formation. $\theta \approx 82°$ for aqueous inner phase, and $\theta \approx 70°$ for oil inner phase.

wetting conditions: one segment of the channel wall is made hydrophobic and the other segment is made hydrophilic. Researchers have to locally modify the wettability of the channel walls for every single chip. This process is always complicated and is unfavorable for further applications in the industry, where mass production with simple and rapid fabrication processes are required. To highlight this point, we extend our single 3D junction to two sequential 3D junctions to generate double emulsions where even more complicated wetting conditions must be maintained. Generated double emulsions are shown in Fig. 2(c)–(e) and also seen in ESI S4–S6,† demonstrating that different double emulsions can be produced by the same chip without any surface treatment of the channel walls. This extension from single 3D junction to two sequential 3D junctions is quite easily achieved through 3D printing technology. However, it is not easy to make this extension using current traditional fabrication techniques. This again demonstrates the flexibility and convenience of 3D printing technology. The liquids we used to generate both modes of double emulsions are listed in Table 1. To the best of our knowledge, this is the first time that different double emulsions can be both produced in the same flow-focusing structure.

An important application for emulsions in microfluidic device is to produce functional particles based on emulsion templates.[38] Variety of chemical reagents are dissolved in either the aqueous phase or oil phase. Therefore, researchers must use different microfluidic devices to generate different droplet templates (water or oil) for functional particle production. Now this low-cost printed chip can be used to produce functional particles based on both water and oil droplet templates without need for changing the chips. Here W/O emulsions are used as templates to produce magnetically responsive microspheres, to demonstrate a potential application for chemical and material engineering. The inner disperse phase consists of poly(ethylene glycol) diacrylate precursor solution (Sigma-Aldrich), together with 5% (v/v) 20 nm nanomagnetic particles solution (Micromod Partikeltechnologie GmbH.) and 2 wt% 2,2-dimethoxy-2-phenylacetophenone (Sigma-Aldrich) as photoinitiator, while the outer continuous phase is 100 cSt silicone oil. Droplets containing nanomagnetic particles are irradiated under UV light for about 5 minutes for polymerization, to form magnetically responsive microspheres. Fig. 7 shows how these magnetically responsive microspheres are attracted to the edge of Petri dish from the center by a magnet.

4 Conclusions

In this paper, we present a design and fabrication of 3D miniaturized fluidic emulsion generator using 3D printing technology. The advantage of having a truly 3D junction, is that unfavorable wettability of the channel-walls does not prevent the emulsion formation.

This 3D junction will be quite complicated and expensive to fabricate using traditional fabrication techniques, but can be

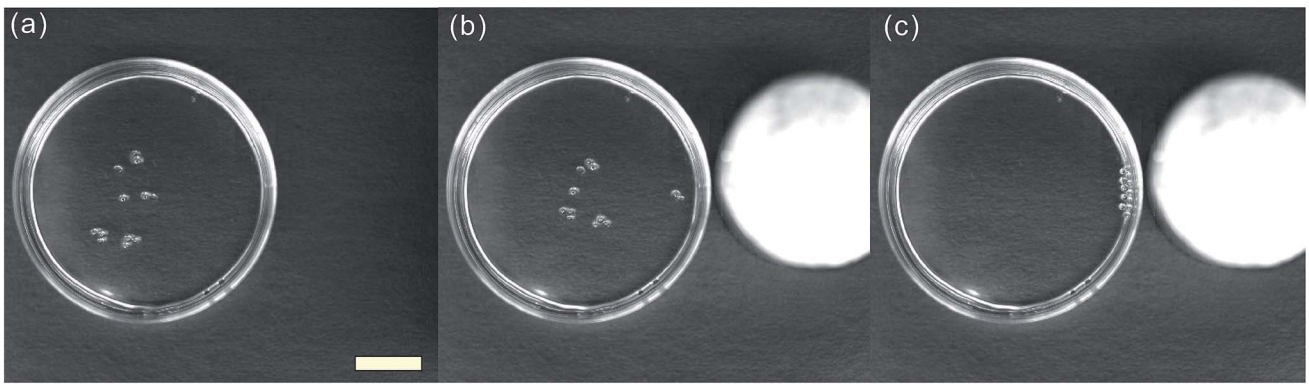

Fig. 7 Functionalized particles fabricated in our 3D printed chip. (a) Magnetically responsive microspheres are dispersed in water inside a Petri dish without applied magnetic field. When a magnet (white circle) is brought near the Petri dish (b), these particles are attracted by the external magnetic field and move towards it (c) until they reach the edge. Scale bar is 10 mm.

easily, rapidly and inexpensively fabricated using the 3D printing method. For the first time, both W/O/W and O/W/O double emulsions can be produced in the same flow-focusing structure without modifications or additional wall wettability treatments. The excellent transparency of our chips is highly favorable for observation and various microfluidic applications requiring optical access.

Uniform scaling laws for both emulsion (W/O and O/W) drop sizes generated in our 3D emulsion generator are successfully proposed for the first time, which provides an excellent prediction and guidance for researchers to produce different sizes of droplet templates for variety of applications using similar 3D flow structures. Our design can be easily extended with more sequential 3D junctions for even higher-order emulsions or be paralleled to produce an emulsion generator array to increase the production rate, which is attractive in the industry field.

We also presented the production of magnetically responsive microspheres based on droplet templates, as an example of functional particle production, showing the great potential of our emulsion generator for chemical and material applications.

3D printing technology is undergoing a rapid development currently. More importantly, this 3D geometry achieved here can be easily extended in a modular manner, which will enable us to produce higher-order composite emulsions regardless of channel wettability. We believe that more and more complex miniaturized fluidic devices will soon be easily fabricated using 3D printing technique with higher resolution and faster speed.

Acknowledgements

Research reported in this publication was supported by King Abdullah University of Science and Technology (KAUST). We also thank Ulrich Buttner for helpful instructions on using the 3D-printer in the KAUST Microfluidics Thrust Area Labs.

References

1 G. M. Whitesides, *Nature*, 2006, **442**, 368–373.
2 A. B. Theberge, F. Courtois, Y. Schaerli, M. Fischlechner, C. Abell, F. Hollfelder and W. T. Huck, *Angew. Chem., Int. Ed.*, 2010, **49**, 5846–5868.
3 H. Song, D. L. Chen and R. F. Ismagilov, *Angew. Chem., Int. Ed.*, 2006, **45**, 7336–7356.
4 D. T. Chiu, R. M. Lorenz and G. D. Jeffries, *Anal. Chem.*, 2009, **81**, 5111–5118.
5 J. I. Park, A. Saffari, S. Kumar, A. Günther and E. Kumacheva, *Annu. Rev. Mater. Res.*, 2010, **40**, 415–443.
6 B. G. Chung, K.-H. Lee, A. Khademhosseini and S.-H. Lee, *Lab Chip*, 2012, **12**, 45–59.
7 D. Dendukuri and P. S. Doyle, *Adv. Mater.*, 2009, **21**, 4071–4086.
8 W. J. Duncanson, T. Lin, A. R. Abate, S. Seiffert, R. K. Shah and D. A. Weitz, *Lab Chip*, 2012, **12**, 2135–2145.
9 S. Seiffert, *Macromol. Rapid Commun.*, 2011, **32**, 1600–1609.
10 J. R. Anderson, D. T. Chiu, H. Wu, O. Schueller and G. M. Whitesides, *Electrophoresis*, 2000, **21**, 27–40.
11 A. R. Abate, J. Thiele, M. Weinhart and D. A. Weitz, *Lab Chip*, 2010, **10**, 1774–1776.
12 A. Abate and D. Weitz, *Small*, 2009, **5**, 2030–2032.
13 A. Utada, E. Lorenceau, D. Link, P. Kaplan, H. Stone and D. Weitz, *Science*, 2005, **308**, 537–541.
14 S.-H. Kim, J. Nam, J. W. Kim, D.-H. Kim, S.-H. Han and D. A. Weitz, *Lab Chip*, 2013, **13**, 1351–1356.
15 S.-H. Kim, H. C. Shum, J. W. Kim, J.-C. Cho and D. A. Weitz, *J. Am. Chem. Soc.*, 2011, **133**, 15165–15171.
16 E. Q. Li, J. M. Zhang and S. T. Thoroddsen, *J. Micromech. Microeng.*, 2014, **24**, 015019.
17 J. M. Zhang, E. Q. Li and S. T. Thoroddsen, *J. Micromech. Microeng.*, 2014, **24**, 035008.
18 L. Yang, K. Wang, S. Mak, Y. Li and G. Luo, *Lab Chip*, 2013, **13**, 3355–3359.
19 K. Wang, L. Xie, Y. Lu and G. Luo, *Lab Chip*, 2013, **13**, 73–76.
20 W. Lan, S. Li, J. Xu and G. Luo, *Mcirofluid. Nanofluid.*, 2012, **13**, 491–498.
21 K. Sun, T.-S. Wei, B. Y. Ahn, J. Y. Seo, S. J. Dillon and J. A. Lewis, *Adv. Mater.*, 2013, **25**, 4539–4543.
22 J. N. Hanson Shepherd, S. T. Parker, R. F. Shepherd, M. U. Gillette, J. A. Lewis and R. G. Nuzzo, *Adv. Funct. Mater.*, 2011, **21**, 47–54.
23 D. Therriault, S. R. White and J. A. Lewis, *Nat. Mater.*, 2003, **2**, 265–271.
24 M. D. Symes, P. J. Kitson, J. Yan, C. J. Richmond, G. J. Cooper, R. W. Bowman, T. Vilbrandt and L. Cronin, *Nat. Chem.*, 2012, **4**, 349–354.
25 E. Li, Q. Xu, J. Sun, J. Fuh, Y. Wong and S. Thoroddsen, *Sens. Actuators, A*, 2010, **163**, 315–322.
26 P. J. Kitson, M. H. Rosnes, V. Sans, V. Dragone and L. Cronin, *Lab Chip*, 2012, **12**, 3267–3271.
27 K. G. Lee, K. J. Park, S. Seok, S. Shin, J. Y. Park, Y. S. Heo, S. J. Lee, T. J. Lee, *et al.*, *RSC Adv.*, 2014, **4**, 32876–32880.
28 A. K. Au, W. Lee and A. Folch, *Lab Chip*, 2014, **14**, 1294–1301.
29 G. Comina, A. Suska and D. Filippini, *Lab Chip*, 2014, **14**, 2978–2982.
30 W. Lee, D. Kwon, W. Choi, G. Y. Jung and S. Jeon, *Sci. Rep.*, 2015, **5**, 7717.
31 L. Donvito, L. Galluccio, A. Lombardo, G. Morabito, A. Nicolosi and M. Reno, *J. Micromech. Microeng.*, 2015, **25**, 035013.
32 A. I. Shallan, P. Smejkal, M. Corban, R. M. Guijt and M. C. Breadmore, *Anal. Chem.*, 2014, **86**, 3124–3130.
33 K. C. Bhargava, B. Thompson and N. Malmstadt, *Proc. Natl. Acad. Sci. U. S. A.*, 2014, **111**, 15013–15018.
34 A. Rotem, A. R. Abate, A. S. Utada, V. van Steijn and D. A. Weitz, *Lab Chip*, 2012, **12**, 4263–4268.
35 B. Wendel, D. Rietzel, F. Kühnlein, R. Feulner, G. Hülder and E. Schmachtenberg, *Macromol. Mater. Eng.*, 2008, **293**, 799–809.
36 A. S. Utada, A. Fernandez-Nieves, H. A. Stone and D. A. Weitz, *Phys. Rev. Lett.*, 2007, **99**, 094502.
37 T. Cubaud and T. G. Mason, *Phys. Fluids*, 2008, **20**, 053302.
38 J.-T. Wang, J. Wang and J.-J. Han, *Small*, 2011, **7**, 1728–1754.